Zoning patterns of Fe and V in spinel from a type B Ca-Al-rich inclusion: Constraints on subsolidus thermal history

J. M. PAQUE[*], D. S. BURNETT, and J. R. BECKETT

California Institute of Technology, Division of Geological and Planetary Sciences, 100-23, Pasadena, California 91125, USA
[*]Corresponding author. E-mail: julie@paque.com

Abstract–We obtained two-dimensional concentration maps for the minor elements Fe and V in 21 spinel crystals in the Allende type B1 inclusion TS-34 with a 4–5 μm resolution. Locally high concentrations of Fe occur along at least one edge of the spinels and decrease toward the center of the grains. Enrichment in V can also occur along edges or at corners. In general, there is no overall correlation of the Fe and V distributions, but in local regions of two grains, the V and Fe distributions are correlated, strongly suggesting a local source for both elements. In these two grains, opaque assemblages are present that appear to locally control the V distributions. This, coupled with previous work, suggests that prior to alteration, TS-34 contained V-rich metal. Oxidation of this metal during alteration can account for the edge/corner V enrichments, but provide only minor FeO contributions, explaining the overall lack of correlation between Fe and V. Most of the FeO appears to have been externally introduced along spinel boundaries during alteration. These alteration phases served as sources for diffusion of FeO into spinel. FeO distributions in spinel lead to a mean attenuation length of ~8 μm and, using literature diffusion coefficients in isothermal and exponential cooling approximations for peak temperatures in the range 600–700 °C, this leads to a time scale for calcium-aluminum-rich inclusion (CAI) alteration in the range of decades to centuries.

INTRODUCTION

Calcium-aluminum-rich inclusions (CAIs) are objects encompassing a rich diversity of bulk and phase compositions reflecting various processes, environments, and times of formation. As probably the oldest igneous rocks in the solar system, they have been studied in considerable detail (MacPherson 2004; MacPherson et al. 1988). Type B1 inclusions are an important subclass consisting mostly of spinel, melilite, fassaitic clinopyroxene, and anorthite with a melilite-enriched outer mantle and variable amounts of fine-grained alteration products. These inclusions are typically spheroidal in shape (but see Caillet et al. 1993) and the coarse-grained phases are generally thought to have crystallized during one or more melting events, interspersed with or followed by alteration of varying intensity at lower temperatures (Beckett et al. 2000; MacPherson and Davis 1993; MacPherson and Grossman 1981; Paque et al. 2000; Stolper 1982). The melting events have received a great deal of attention because of their potential for constraining physical processes and high-temperature environments in the primitive solar nebula. Metasomatic events may have left equally powerful clues to the evolution of our solar system

but the emphasis to date has been on characterizing the basic alteration reactions (McGuire and Hashimoto 1989; Nomura and Miyamoto 1998; Wark 1981) and the issue of asteroidal versus nebular sources for the inferred elemental fluxes (Krot et al. 1995). There are few quantitative constraints on either the thermal histories during alteration or the nature of the altering medium.

Several things happen during secondary processing of a type B1 inclusion. Some reactions are thermally activated. For example, monticellite plus grossularite can form by the reaction of melilite and anorthite (Hutcheon and Newton 1981). Generally, however, the alteration process is dominated by open-system reactions involving magnesian melilite and vapor or aqueous solutions that yield a complex mixture of grossularite, monticellite, and wollastonite (Davis et al. 1994) and/or nepheline (Nomura and Miyamoto 1998). This leads to a net increase of Na and Si in the bulk inclusion and, probably, a decrease in Mg (e.g., Wark 1981). Alloys, which are present in small amounts, were generally oxidized or sulfidized (Blum et al. 1989). Aluminous melilites, fassaites, and igneous anorthites (Davis et al. 1994; Steele et al. 1997) are less affected.

Spinel is a special case. This phase did not break down

during the alteration process(es) but, near inclusion rims, crystals commonly show a characteristic Fe enrichment (e.g., Kurat et al. 1975) and even spinels from inclusion interiors usually have minor-element concentrations readily measurable by electron microprobe microanalysis (EPMA) (Connolly and Burnett 1999; Taylor and McKeegan 2004). It is generally believed that alteration event(s) lead to the introduction of oxidized iron, more extensively in the rim, but also in regions throughout the interior of the inclusion as the solubility of Fe in spinel is negligible under the highly reducing conditions of CAI crystallization. Other elements may have been similarly affected so that chemical signatures of high-temperature events in spinel are overprinted at lower temperatures (Connolly et al. 2003; Meeker et al. 1983). If spinel is to be used in constraining the nature of environments in the early solar system, then it is very important to first understand which processes contributed to the observed elemental distributions.

Connolly and Burnett (1999) and Connolly et al. (2003) analyzed a large number of spinels in Allende type B1 inclusions TS-23 and TS-34 using EPMA and concluded that grains were consistently zoned, with FeO increasing from core to rim. In contrast, FeO concentrations in spinel from a Leoville type B1 inclusion (Connolly and Burnett 1999) were substantially lower and grains were not obviously zoned. The authors attributed these effects to the introduction of Fe during alteration of all three inclusions, leading initially to zoned grains, but subsequent heating homogenized the Leoville grains. If concentration profiles for FeO in the spinel of type B1s reflect the diffusive response to chemical potentials imposed on grain surfaces during alteration, then where zoning is present, as in TS-34, the distribution of FeO holds information on the thermal history, which can be extracted in part from concentrations within a spinel grain, given suitable diffusivities (e.g., Liermann and Ganguly 2002). Where zoning is absent, as in the Leoville spinels, it may still be possible to place some constraints on the nature of previous alteration events based on average concentrations of Fe and differences in concentration between grains, although this is not attempted in this paper.

While significant Fe concentrations in spinel are thought to reflect low-temperature processes, the origin of V distributions is less clear. Connolly et al. (2003) and Taylor and McKeegan (2004) emphasized the possible role of multiple melting events in producing the observed distribution in Ti-V concentrations of spinels from TS-34, but Armstrong et al. (1987) saw V distributions in another Allende inclusion as reflecting mostly secondary effects. Thus, the extent to which V distributions in CAI spinels record high- and/or low-temperature processes remains an open question.

Unraveling the contributions from various processes to the observed elemental distributions in spinel requires detailed characterization of zoning patterns. Unfortunately, spinel grains in most type B1s are small, typically 10–15 μm

across in section, making it difficult to do much more than establish approximate concentration differences between core and rim. There are, however, some important exceptions. Armstrong et al. (1987) measured Fe concentrations along a 40 μm traverse in a large spinel grain from the Allende-type B1 inclusion Egg 6. They modeled the profile using diffusion coefficients from Freer and O'Reilly (1980) and obtained quantitative constraints on the thermal history of the inclusion. The inferred conditions are incorrect because the experimentally determined diffusivities they used were in error and they only considered constraints at high temperatures relevant to melting of the host CAI. Nevertheless, they clearly demonstrated the potential for using large zoned spinel crystals to establish constraints on the thermal histories of CAIs. Connolly et al. (2003) studied TS-34, an inclusion with spinel grains as much as 150 μm across. In this study, we use the same section Connolly et al. (2003) analyzed but concentrate on a determination of detailed concentration maps of individual spinel grains and relationships between zoning of minor elements in the spinel and the nature of surrounding phases. Our objective is to better understand the origin and evolution of minor element distributions among and within spinels of this inclusion and to thereby establish constraints on the evolution of the host CAI and its significance to nebular and planetary body evolution. A preliminary report on the work presented in this study is given by Burnett et al. (2004). Titanium data, which we acquired at the same time, are to be presented elsewhere.

SAMPLES AND ANALYTICAL PROCEDURES

We utilized the same polished section of a large (1.2 cm in diameter) type B1 CAI from Allende previously used by Connolly et al. (2003) and distinguish three basic styles of occurrence for the spinel: 1) "isolated" grains, in which there are no edges shared with other spinel grains in the plane of the section, although some may be connected to other spinel grains in the third dimension; 2) "sutured" crystals that share one or more edges with other spinel grains in the plane of the section, and therefore one or more edges or faces in three dimensions; and 3) spinel-bearing portions of the Wark-Lovering rim (Wark and Boynton 2001; Wark and Lovering 1977). In this work, we describe analytical data for the first two textural settings, isolated and sutured spinel crystals in the core and mantle of TS-34. In TS-34 we have not found the V-rich magnetite associated with Fremdlinge or opaque assemblages found in other Allende CAIs (Blum et al. 1989; El Goresy et al. 1978). Our focus is on Mg-rich spinels for which concentrations of Fe expressed as FeO are less than, and usually much less than, 1 wt%.

Table 1 provides a summary of the local petrography for each of 21 analyzed spinel crystals. Targeted grains ranged from 30 to 105 μm across and were initially identified based on a large (approximately 60 × 60 cm) image of the inclusion

Table 1. Summary of the local petrography for each of 21 analyzed spinel crystals.

Spinel	Location	Type	Host mineral	Approximate size (μm)[a]	Number of points analyzed	Number of spinel points	%	Notes[b]
A1	Mantle	Individual	Melilite	100 × 75	303	192	63	a, b, d, k, l
A2	Mantle	Individual	Melilite	65 × 65	319	145	45	i, k
A8	Mantle	Individual	Melilite	47 × 35	141	62	44	a, b, e, h, i
A9	Mantle	Individual	Melilite	70 × 53	252	177	70	a, f, i
D1	Mantle	Individual	Melilite	33 × 33	110	37	34	a, i
Sp5	Mantle	Individual	Melilite	53 × 53	100	62	62	d, i
A6	Core	Individual	Cpx/mel (+alt)	65 × 53	198	91	46	e, i
A12	Core	Individual	Melilite	80 × 80	307	237	77	c
B1	Core	Individual	Mel (+alt)/cpx	48 × 45	180	105	58	c, e
B2	Core	Individual	Melilite	66 × 66	276	184	67	h
B3	Core	Individual	Cpx	80 × 70	409	247	60	
B4	Core	Individual	Melilite	62 × 62	198	143	72	c
Sp14	Core	Individual	Core cpx	100 × 90	346	219	63	g
A4	Core	Sutured	Cpx	A: 105 × 88	566	365	65	b, d, j, k
			Melilite	B: 75 × 70				
A5	Core	Sutured	Cpx	80 × 60	244	110	45	b
E1	Mantle	Sutured	Melilite	58 × 58; 88 × 70	615	285	40	h
E2	Mantle	Sutured	Melilite	33 × 31; 59 × 44; 44 × 41	374	233	62	i

[a]Approximate size of grain exposed in thin section, measured along perpendicular axes.

[b]a = No vanadium analyses available; b = opaque assemblage along one edge; c = melilite grain surrounding spinel is altered; d = metal grain included in spinel; e = metal/sulfide grain(s) along edge(s); f = alteration veins around grain; g = micron-size perovskite and Ni-rich sulfides along edge; h = blebs of cpx adjacent to spinel; i = thin rind of cpx along portion of spinel rim; j = no cpx adjacent to spinel in thin section; k = cpx inclusion in spinel; l = refractory metal nugget (RMN) inclusion in spinel.

constructed from low-magnification photomicrographs obtained using a JEOL 733 scanning electron microscope (SEM). Those grains selected for study were taken from among the largest examples for each textural setting and host phase. Nine are isolated inclusions in melilite with varying degrees of alteration, six from the mantle and three from the core of TS-34. Two isolated grains are wholly included in clinopyroxene and two others were selected because they lay on grain boundaries with fassaite enclosing one portion of the grain and melilite ± alteration products enclosing the rest. The other eight grains we analyzed are members of sutured sets, two of which are wholly included in melilite, one wholly included in clinopyroxene, and one bounded by both melilite and clinopyroxene phenocrysts.

Concentrations of Fe, Si, and V were determined by high-precision electron microprobe analyses using the JEOL 733 Superprobe at Caltech, but we acquired V data for only 17 of 21 grains due to a spectrometer failure. Standards included V_2O_3 (V) and fayalite (Fe, Si). Magnesium and Al were fixed to stoichiometric spinel ($MgAl_2O_4$) values to allow matrix corrections of the data. The beam diameter was 2–3 μm, which, based on Monte Carlo simulations, leads to an activation volume approximately 3–4 μm across at its maximum for our operating conditions (200 nA beam current, 100 s count time, 15 kV accelerating voltage). Detection limits for most analyses are 0.003 wt% for V, and 0.006 for Fe with typical 1σ counting statistics errors of 1.6% for V and 6.1% for Fe. Unless otherwise stated, all errors quoted in this work refer to 1 standard deviation.

Analyses were performed over a grid pattern to cover spinel and the immediately adjacent area with a typical step size of 4 or 5 μm between analyses, which was sufficient to avoid overlapping activation volumes for adjacent points. Analyses with concentrations of SiO_2 exceeding 0.1 wt% were rejected as not accurately reflecting spinel, although we used such compositions to help identify the contaminating phase and to define boundaries of the spinel grain within the analyzed grid. Typically, 150–300 data points were obtained on each spinel grain, of which 34–70% were deemed to be uncontaminated spinel. Only a small fraction of these data are given explicitly in this work but complete data sets are available upon request from the authors.

In this work, we calculate Fe in spinel as FeO and V as V_2O_3. The actual valence states are generally unknown but, where concentrations are high enough for stoichiometry arguments to be used (e.g., Armstrong et al. 1987), Fe is divalent and most if not all of the V is trivalent. To our knowledge, there are no direct constraints on the oxidation state of V and Fe in most CAI spinels, but the presence of Fe^{3+} in the magnetite of opaque assemblages (Armstrong et al. 1985) and of V^{2+} in clinopyroxene (Sutton et al. 2002) in CAIs should serve as a reminder that valence states other than the ones we selected are possible.

RESULTS

We begin with a discussion of general features of Fe-V zoning as exemplified by representative isolated grains

included in melilite and fassaite and then show that essential features of the concentration maps can be captured through profiles taken across the grains. The use of these profiles provides a simple semi-quantitative way to approach the data from multiple grains. We first apply this approach to isolated grains and then consider sutured spinels.

Element Distribution Maps of Isolated Grains

Figure 1 shows an SEM image of spinel grain B2, an inclusion in melilite from the core of TS-34, and corresponding color-coded concentration maps of Fe and V distributions calculated as FeO and V_2O_3. Profiles, also shown in the figure, are discussed below. The FeO concentration map shows two source regions located at corners of the grain, which in 3-D implies either a vertex or, more likely, an edge. There are also Fe-rich areas shown as pink; these are nominally in the surrounding melilite but background levels of FeO in this phase are so low, <0.04 wt%, that the enrichment is probably associated with local regions of alteration or Fe-rich precipitates along the grain boundaries of spinel. The top vertex shows a similar pattern and, based on the distribution (green versus blue in Fig. 1), the leftmost corner also has enhanced Fe concentrations relative to the lowermost vertex. The lack of clean resolution between the green and blue points reflects the relatively low FeO concentrations and consequent high errors (2σ ~12%). The silicate external to the spinel has a similar distribution in that Fe-rich silicates are associated with nearby Fe-enriched spinel and the Fe-poor silicates are found around the Fe-poor spinel. The V_2O_3 concentration map in Fig. 1 clearly shows that V is enriched in one quadrant relative to the rest of the grain with the lowest concentrations along an opposing edge. The total variation is real but not large (~8% versus errors based on counting statistics approaching 2%) leading to imperfect color resolution. This type of edge/corner V_2O_3 enrichment is found in most, but not all isolated grains. Note that the most V-enriched corner is also the lowest in Fe. A lack of connectivity between V and Fe zoning is endemic in our suite of grains.

Figure 2 shows a backscattered electron (BSE) photomicrograph and color-coded concentrations of FeO and V_2O_3 in spinel grain sp14, which is wholly included within clinopyroxene from the core of TS-34. This grain has two prominent fractures running across it, one filled with alteration products and the other empty, but, at the level of detail allowed by the color map, neither crack affects the overall distribution of minor elements within the grain. We revisit the cracks below as part of a more detailed discussion of this grain but ignore them for present purposes. From Fig. 2, high Fe contents are observed along edges of sp14 with a systematic decrease of FeO toward the center of the grain and toward one corner where SEM observation shows no obvious Fe source (such as an oxide) in the plane of the

section. The surrounding clinopyroxene is FeO poor, <0.04%, and, based on SiO_2 concentrations and high-resolution examination of the spinel-clinopyroxene interface, the Fe-rich edge material is probably an oxide.

The V_2O_3 concentration map for sp14 in Fig. 2 is qualitatively similar to that for grain B2 in Fig. 1, although concentrations are generally lower in grain B2. Concentrations along one edge are substantially higher than the others. A repeated pattern of edge/corner-enriched V distributions occurs in spinel independent of host phase or location within TS-34.

Profiles of Isolated Grains

General patterns of elemental distributions can be ascertained through an examination of crudely contoured concentration maps as shown in Figs. 1 and 2 and the associated description given above. In order to capture the essential features of the two-dimensional distributions of minor elements in spinel, we selected one or more profiles for each oxide taken across each grain. Most of the profiles pass through the minimum and maximum concentrations of an oxide but some were chosen in different orientations to illustrate specific features of the data. Where variations in concentration along the profile significantly exceeded counting statistics, individual data points within a few μm of the profile line were projected onto the line and the concentration used without correction. For V_2O_3, ranges in concentration sometimes approached errors due to counting statistics and we resorted to averaging multiple points adjacent to the profile to produce a single point "on" the profile. This had the effect of smoothing the data. Usually two to six points were averaged but in one case we used five to 12 analyses per profile point. Rolling averages were avoided. Where multiple analyses were used, we computed errors from the standard deviation of the averaged data used to produce the profile point. Usually, these errors approximated those expected from counting statistics but occasionally, larger errors were encountered, indicating real variability in the data points whose concentrations were being averaged. The section we studied was optically thick and grains were selected for analysis on the basis of size, not shape, so we have few direct constraints on where the plane of the section is relative to the center of a crystal in 3-D. Choosing minimum and maximum concentrations to anchor profiles in isolated spinel crystals that were selected to maximize areas in section means that the profiles may reflect contributions from more than one face, and almost certainly require angles substantially off-perpendicular (i.e., distances measured in section from the closest vertex or edge in 2-D exceed the distance to the closest face in 3-D). This has the effect of reducing concentration gradients.

Figures 1 and 2 show oxide concentration profiles for grains B2 and sp14 taken along linear traverses as indicated
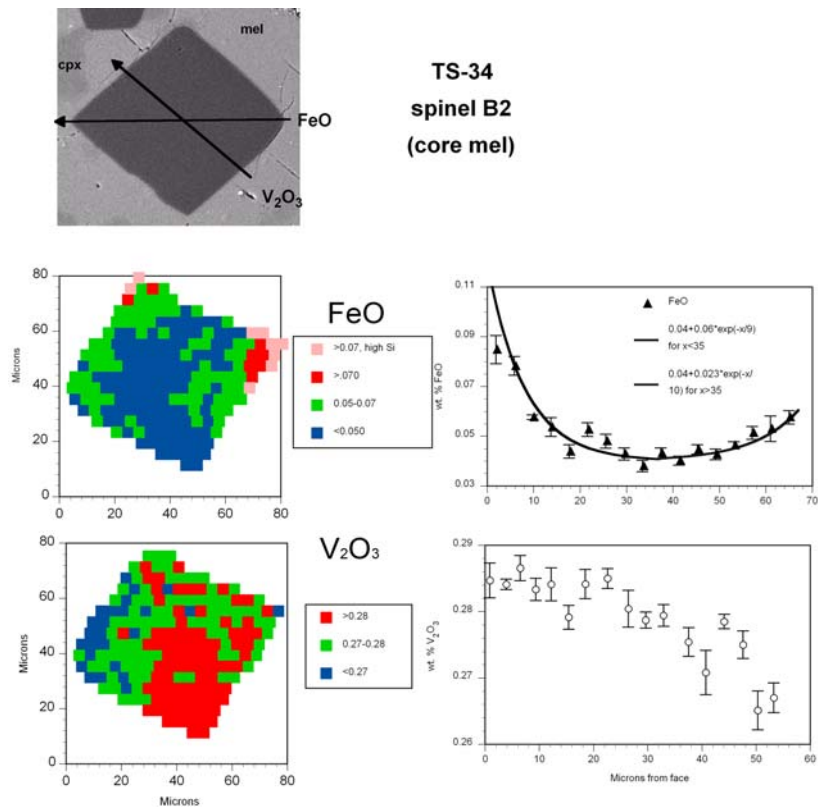
Fig. 1. Spinel grain B2, which is wholly included in melilite (mel) from the core of TS-34. A backscattered electron (BSE) image of the grain (field of view = 80 μm) is shown together with corresponding color-coded concentration maps for wt% FeO and V_2O_3, and concentration as a function of distance along the profiles as indicated on the SEM image where arrows show the direction of increasing distance for the profiles. The pink areas in the FeO map refer to high SiO_2 regions outside spinel. Note that each oxide has a unique distribution pattern. FeO is enriched at two of the vertices and V_2O_3 at a different vertex. For FeO, concentrations fall exponentially from surface-to-center of the grain (equations for curve given in the panel).
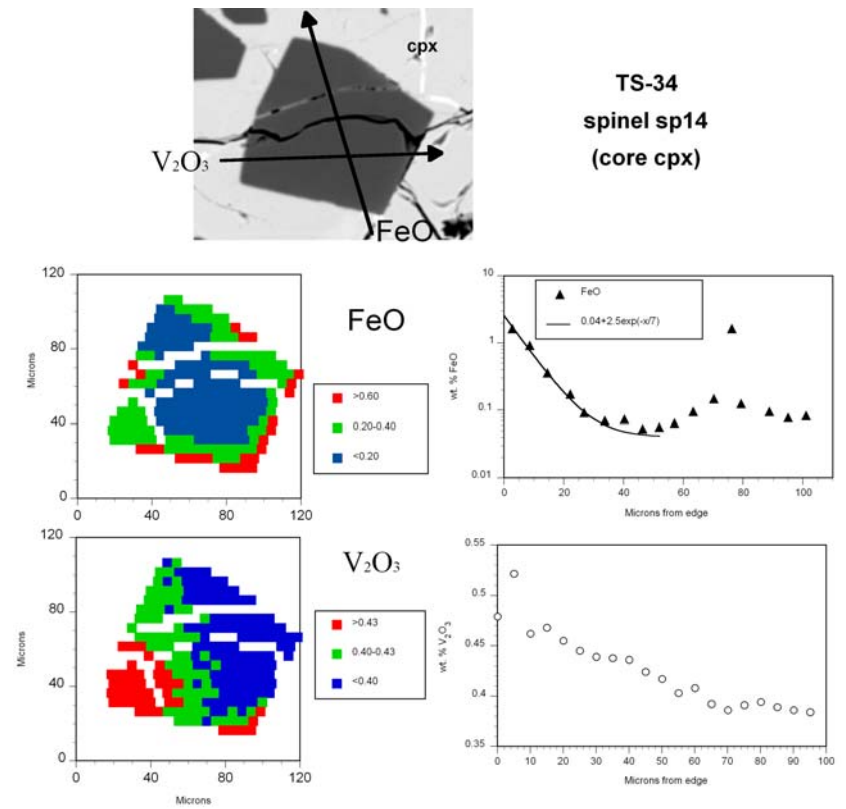
Fig. 2. TS-34 spinel grain sp14, wholly included in clinopyroxene (cpx) from the core of TS-34 with a BSE image (field of view = 120 μm), color-coded concentration maps for wt% FeO and V_2O_3 and concentrations (wt%) of FeO and V_2O_3 as a function of distance along the profiles indicated in the BSE image with arrows pointing in the direction of increasing distance. Points at which the profile path for FeO intersects a crack and an alteration filled vein are also indicated. Note that concentrations of both oxides exceed their counterparts in B2.
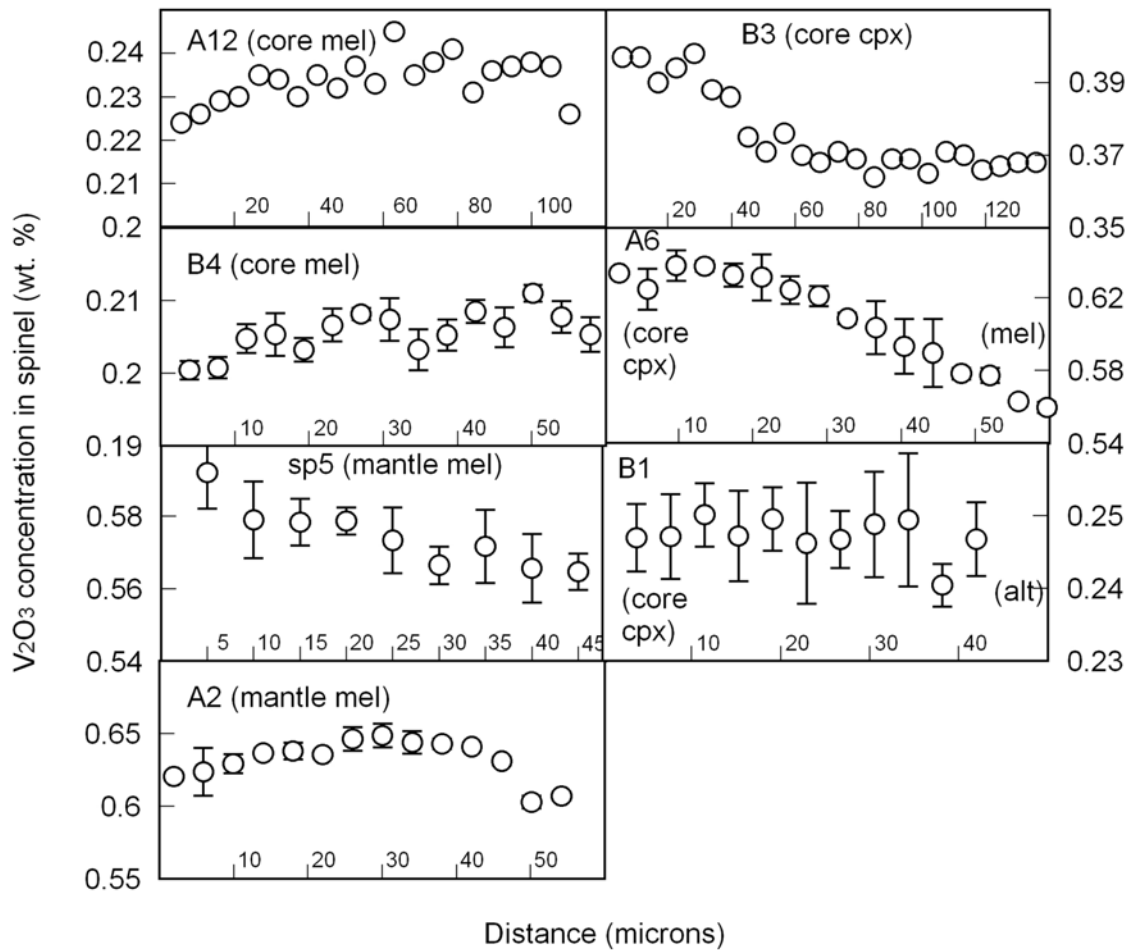
Fig. 3. V_2O_3 profiles for isolated spinel grains in TS-34. Host phases include core (A12, B4) and mantle melilite (sp5, A2) and/or alteration products (B3). Spinel grains A6 and B1 are partially enclosed by melilite or melilite-derived alteration products and partially by clinopyroxene. Note that concentration and spatial scales vary from panel to panel. Error bars, shown where they exceed the symbol size, refer to the population of analyses used to derive each plotted point (see text).

on the BSE photomicrographs. The FeO profiles are well described by a simple exponential function, $C(x) = C_o + C_1 \exp(x_o/x)$, where $C(x)$ is the concentration of the element at position x and C_o, C_1, and x_o are constants, from two sides of the crystal in the case of B2 (Fig. 1). In Fig. 2, the FeO profile crosses two cracks, one empty and the other filled with Fe-rich silicate ± oxide. There is no significant perturbation of the profile in the vicinity of the empty crack. In contrast, the filled vein has a locally significant effect on FeO concentrations. The high FeO points associated with the vein are adjacent to points rejected because of high SiO_2 (i.e., the source of Fe in the analysis volume is either a silicate or an oxide intimately associated with silicates). The points shown in the profile with increasing FeO toward the vein pass the silica rejection test. The edge/corner peaking suggested by the concentration maps of the V_2O_3 distributions is also clear in the profiles.

The FeO profiles shown in Figs. 1 and 2 are typical of those obtained for other isolated spinel grains. Values of C_o

and x_o for the grains we analyzed average 0.05 wt% and 8 μm, respectively, and range from 0.01 to 0.07 and 4 to 14. As discussed below, these parameter values are a measure of initial concentrations (and/or off-center sectioning) and homogenization distances. For one grain, A9, FeO concentrations were chaotic, apparently due to contributions from multiple localized sources and we were unable to fit the profiles.

Figure 3 shows V profiles analogous to those in Figs. 1 and 2 for a variety of petrographic settings. V_2O_3 profiles are more complex than those for FeO but the variations are only 5–10%. Maximum concentrations for most grains occur at corners or along edges but the profile for grain A2 is center-peaked while B1 may be uniform. Variations in V concentrations across grain A6, partially enclosed by clinopyroxene at one end and by melilite/alteration products at the other, are approximately linear.

Our description of the data has thus far been focused on what the profiles show. It is also important to emphasize what
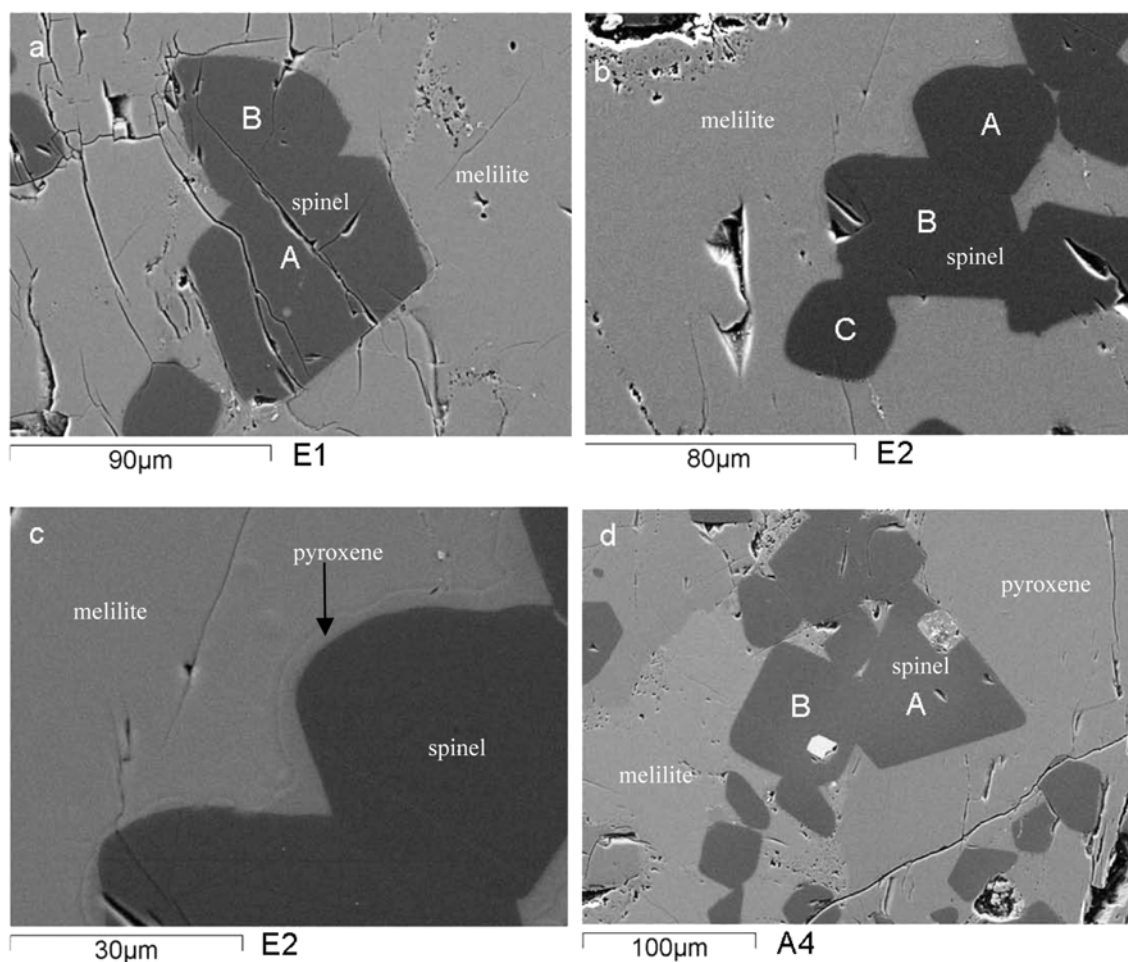
Fig. 4. BSE photomicrographs of sutured sets of spinels in TS-34. Scale bars are included below each panel and individual analyzed grains are labeled (cf. Table 1). a) Sutured set E1, wholly included in mantle melilite. b) Sutured set E2, wholly included in mantle melilite. c) A closeup of the interface between melilite and spinel grains E2A and E2B showing clinopyroxene blebs. d) A4 from the inclusion core. Grain A4A is hosted primarily by clinopyroxene and A4B by melilite. The mottled object partially included in A4A is a very fine-grained, sulfide-rich opaque assemblage (see text). The bright inclusion in A4B is an opaque assemblage consisting of Ni-rich alloy and phosphide.

they don't show. For example, one clear petrographic distinction between spinels in core versus mantle melilites is that the latter generally have a continuous (1–3 μm thick) rind of clinopyroxene along one or more edges and some discontinuous blebs (Paque et al. 2005). Clinopyroxene also occurs at surfaces of spinel grains enclosed in core melilite, but as sparse blebs that cover a small fraction of the grain surface. The boundary clinopyroxenes appear to affect neither the Fe nor V distributions. Similarly, we found FeO distributions for spinels in different petrographic settings to be indistinguishable. In particular, there was no simple correlation between Fe content and distance from the rim of the inclusion or to the nearest large alteration region in the plane of the section indicating, perhaps, that the extent of penetration of Fe into the interior of the inclusion was highly path-dependent. It is also worth re-emphasizing that the positions of hot spots, or regions of V and Fe enrichments, in spinel are usually not correlated.

Sutured Grains

Many spinel grains occur as isolated grains in section, but doublets, clusters, and chains, in which one or more edges of a spinel grain is shared with neighboring spinel crystals, are also common. We analyzed spinels from four sutured sets in TS-34 (Table 1), and Fig. 4 shows BSE images of three examples. E1 and E2 are entirely enclosed in mantle melilite. E1 (Fig. 4a) represents a pair of sutured grains, E1A and E1B, which have empty fractures and an alteration-filled vein reminiscent of those in sp14 (Fig. 2). Rare micron-size (relict?) perovskite grains are present in both E1A and E1B. E2 (Figs. 4b and 4c) is a relatively straight three-grain segment (E2A, E2B, and E2C) of 30–60 micron-size sutured grains in a much longer irregular spinel chain (not shown in Fig. 4). Figure 4c shows a close-up of portions of E2A and E2B showing bounding clinopyroxene between the spinel and host melilite. A4 (Fig. 4d) is a seven-grain cluster of sutured
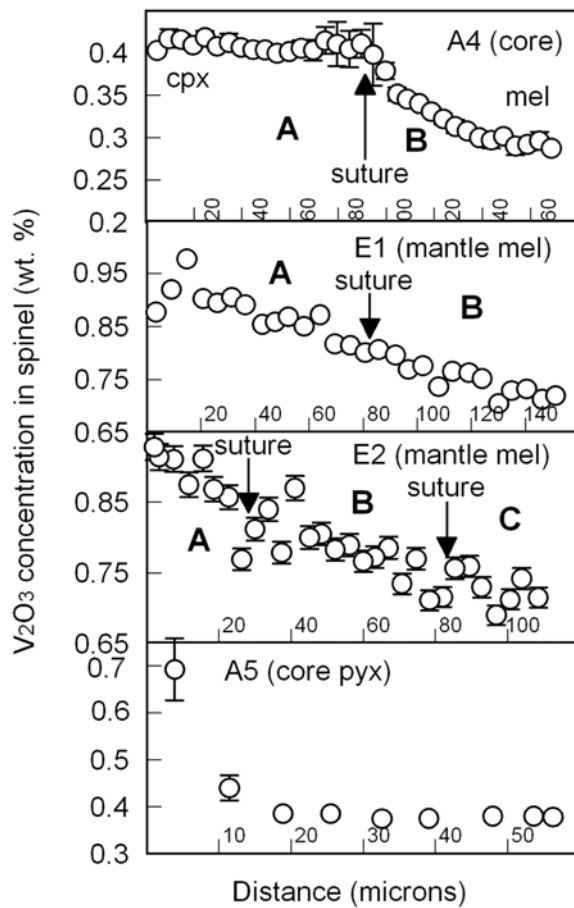
Fig. 5. V_2O_3 profiles for sutured sets of spinel grains in TS-34 taken perpendicular to sutures whose positions are noted, except for A5, for which only one grain was analyzed. Note that both concentration and distance scales vary from panel to panel.

spinel grains in the core of TS-34, of which we have analyzed the two largest. The larger of the mapped grains, A4A, is almost completely surrounded by clinopyroxene. Grain A4B is bounded on one side by grain A4A and is otherwise surrounded by altered core melilite and small spinel crystals. Both A4A and A4B contain opaque assemblages. The opaque assemblage in grain A4A embays the surface and is approximately 20 μm. It bears a superficial resemblance to, but is much smaller than, the "sulfide-rich Fremdlinge" of Armstrong et al. (1987). Mineral identification is difficult because the object is composed of complex, fine-grained material with a maximum grain size of ~4 μm. The cleanest X-ray spectra suggest the presence of forsterite and Ca phosphate. Ni-rich metal is present and sulfide is abundant. Grain A4B contains a Ni-rich metal inclusion, about 20% of which is Fe-Ni-phosphide. Although we have not attempted a detailed study, the lack of oxidation or sulfidization may reflect armoring by spinel, and the opaque assemblage may therefore be representative of an original Fe-Ni-P liquid or alloy/phosphide mixture as it existed prior to incorporation in the spinel.

An important feature of data for the sutured spinels is that FeO concentrations show no perturbations as they cross the trace of the suture between grains. This implies that formation of the suture predated generation of the FeO profile. As noted above with isolated grain sp14, perturbations are generally observed where profiles cross alteration-filled veins but not empty cracks.

V_2O_3 profiles for sutured grains are shown in Fig. 5. There appears to be a discontinuity at the suture for A4, but the sutures in E1 and E2 are not associated with significant perturbations in composition. Both E1 and E2 show V_2O_3 concentrations generally decreasing from one end of the profile to the other. We acquired data for only one grain in sutured set A5. V_2O_3 is enriched along one edge with concentrations dropping toward the interior by a factor of two within ~20 μm.

Summary of Observations

Based on the above discussion, we can make the following generalizations concerning FeO and V_2O_3 distributions in spinel from TS-34.

1. In all grains, locally high concentrations of FeO occur along at least one edge (probably a face in 3-D) and decrease toward the center of the grains. This almost certainly reflects the incorporation of external FeO in an alteration event(s) and simultaneous and/or subsequent diffusion of FeO into the spinel.

2. At least two generations of cracks are present in spinel grains. Filled cracks are often associated with significant perturbations in FeO profiles while open cracks show no effect on concentration profiles.

3. Most spinel grains show V-enrichment near one corner or along one edge. Occasional core enrichments also occur.

4. There is no overall correlation between the two-dimensional distributions of FeO and V_2O_3.

5. Where melilite/alteration encloses a spinel grain at one end of the crystal and clinopyroxene the other, concentration profiles of V_2O_3 are approximately linear between the two ends, decreasing from clinopyroxene to spinel.

6. Opaque assemblages can have a significant effect on elemental distributions in spinel if they are exposed at the surface of the grain but may be essentially inert if entirely enclosed by spinel. The latter suggests that volume transport of O_2 through the spinel grains was inefficient.

DISCUSSION

In considering V and Fe distributions, the major objectives are to sort out regional from local sources and to determine the extent to which processes that produced the V and Fe distributions might be connected. We discerned no

global correlation between the distributions of the two elements, but this does not mean that the same process acting on different sources wasn't involved in both.

Origin of the Edge/Corner-Peaked V Distributions and Relationships among Minor Elements in Spinel

The range of variation in V_2O_3 within spinel grains is relatively small (from 0 to 25%) (Figs. 1–3) and enrichments are generally at corners or along edges. With important exceptions, Fe and V distributions are uncorrelated. We first consider why zoning of V and Fe are sometimes correlated with each other and then why they generally are not.

A4 (Fig. 4) appears to be a very small-scale version ("microZelda") of the spinel grain described by Armstrong et al. (1987), in which large-scale, correlated enrichments in FeO and V_2O_3 are observed associated with an opaque assemblage. Small regions enriched in V can be seen at the margins of the opaque assemblage at the edge of grain A4A. Also, the interior metal/phosphide in grain A4B has detectable V. Thus, the opaque inclusions in both A4A and A4B appear to be V sources. Grain A5 (not shown in Fig. 4) contains an opaque assemblage along an edge that is the apparent source of zoning in both FeO and V_2O_3.

We found none of the V-rich magnetite or clinopyroxene that are conspicuous phases in the Armstrong et al. example, but their conclusion that V-enriched metal was the ultimate source of alteration phases and Fe-V zoning in the spinel is consistent with our observations.

The FeO distribution in the sutured grain A4 is complex. There is a thin FeO-rich border around both opaque inclusions, but the peak of the FeO distribution is on a line between the two opaque assemblages, indicating that the major FeO source is out of the plane of the section. Neither the oxidized opaque assemblage in A4A nor the metal phosphide grain in A4B appear to be the major source of the FeO in grain A4A. The peak FeO concentration is about 5 wt%, among the highest amounts we measured, certainly the highest for the interior of a spinel. The melilite boundary of grain A4B is FeO-free, and a general gradient across grain A4B from the FeO in grain A4A is observed.

Where opaque assemblages interact with adjacent spinel, local Fe and V distributions may be correlated, as observed in spinels near Zelda (Armstrong et al. 1987) and in grains A4 and A5 from this study, although for the latter pair the principal source appears to be out of the plane of the thin section. Since the Fe and V must be oxidized before they can be redistributed from a metallic phase to spinel, it seems likely that the Fe-V enrichments in spinel associated with opaque assemblages reflect the same oxidation event. On the other hand, where the oxidizing medium lacks access to an opaque assemblage, as appears to be the case for a metal grain enclosed in spinel grain A6, there will be little or no enrichment in the surrounding spinel.

Spinel grains A4 and A5 are exceptional in that Fe and V distributions are partially correlated and the sources appear to be local. Most of the time, this is not the case. Both V_2O_3 and FeO show edge or corner enrichments (e.g., Figs. 1 and 2) but the enriched portions tend to be in different parts of the crystal. Fe sources are generally more regional, and with the occasional exception of an oxidized opaque assemblage, Fe was transported into the CAI from outside. Even in grain A4A where Fe and V distributions are correlated, it is only an increment of V added that stands out in the V map and correlates with the Fe distribution. This is consistent with the idea that V and Fe distributions are partly connected and partly independent. The A4 profiles in Fig. 5 refer to a region away from the opaque inclusions. Thus, Fig. 5 shows the Fe independent part of the V distribution.

Overall, we suggest that the V distributions reflect two different components. There is a relatively high temperature component that reflects equilibration with local crystalline silicates and/or liquids. This leads to the overall correlation of Ti and V among spinel crystals and the correlation between V concentrations in spinel and co-existing clinopyroxene observed by Connolly et al. (2003). Our observations are consistent with either uniform or center-peaked V concentration profiles within pre-alteration spinel grains, although grain-to-grain variability was present (Connolly et al. 2003). Out-of-plane sources of oxidized V plus sectioning effects in general can explain the variety of V profiles shown in Fig. 5.

At a later time under more oxidizing conditions, some V is mobilized locally through oxidation of metal grains or other sources. This same event produces local mobility in Fe from some opaque assemblages. This is accompanied by a larger scale, generally more pervasive, FeO mobility through a medium that was responsible for the overall alteration of the inclusions. For the purposes of this discussion the source of FeO could be either the solar nebula or the Allende parent body. The silicate/oxide alteration phases (e.g., Fig. 1) are the sources for subsequent diffusion of FeO into spinel. This later oxidation event(s) produces the observed variations in V but since the perturbations in concentration are within a few per cent of the mean concentrations of the grains, previously established inter-grain correlations between V and Ti in spinel and of V between spinel and coexisting clinopyroxene remain. The general lack of correlation between V and Fe zoning reflects the local nature of the perturbing V sources and mixed local and regional origin of oxidized Fe.

The gradient of V in spinel A6 (Fig. 3) from the clinopyroxene boundary toward the melilite suggests that diffusion of V from clinopyroxene into spinel might be occurring. If, however, this was an important controlling effect for spinel V distributions, then an overall edge peaked distribution would be observed for spinel inclusions completely in clinopyroxene; Fig. 2 shows that this is not observed. The fact that the high point in the A6 profile is

adjacent to clinopyroxene probably means that the V source just happened to be on the clinopyroxene-spinel boundary.

A possible problem for our model is that V edge/corner enrichments are found in essentially every spinel, but opaque inclusions are relatively rare. However, if the effective V migration length from a source is 30–50 microns and the sources (based on A4) are 5–10 microns in diameter, then a relatively low density of sources will suffice and the probability of sectioning one will be low. Moreover, it may be that most of the V-rich metals or other sources were small and/or located on grain boundaries, and have been totally reacted, unless armored by being spinel inclusions as in grain A4. We conclude that the relative rarity of opaque inclusions in spinels is not problematic for our preferred interpretation.

Cracks

As noted above, we distinguished two types of cracks in the spinels we analyzed. Some are empty while others are filled with Fe-bearing alteration material (e.g., Fig. 2). Iron zoning profiles in spinel show no significant perturbations as they cross empty cracks whereas filled veins have a locally significant effect. We interpret this to mean that empty cracks postdate the alteration process. Filled cracks occurred prior to or during alteration and, in principle, their distribution and abundance reflects earlier shock/thermal events.

Constraints on Thermal History

The best constraints on time scales for the alteration process are obtained by combining our data with literature determinations of diffusivities and estimates of the temperatures of CAI alteration. We first consider available constraints on the temperatures at which alteration processes occurred and then show how these temperatures play out in the thermal history of TS-34.

Temperature of Alteration

Modification of the originally igneous phases in TS-34 probably took place over a substantial range in temperature but there are some constraints on specific processes. For example, Hutcheon and Newton (1981) noted that grossularite is unstable above about 800 °C at low pressures, which restricts the formation of this common alteration phase to lower temperatures. They also calculated that the formation of grossularite and monticellite from anorthite and melilite occurs at a temperature of 668 °C. Barber et al. (1984) infer an alteration temperature for type B1 melilite of about 650 °C based on a homologous temperature argument wherein temperatures were high enough for bulk diffusion to dominate but low enough for diffusion along pipe dislocations to still be important. Armstrong et al. (1987) obtained temperatures of 600–800 °C based on magnetite-sulfide equilibria in opaque assemblages and Blum et al. (1989) showed that

PGE-enriched alloys in opaque assemblages equilibrated at ~500 °C and that oxidation to form them must therefore have occurred at or above this temperature. None of these constraints comes from TS-34 itself but all are applicable to Allende type B1 inclusions. Overall, temperatures of 600–700 °C appear reasonable for the major alteration reactions in TS-34 and, to the extent that transport of Fe to spinel grains and diffusion into them occurred during alteration, this also constrains the diffusion process for FeO in spinel to similar conditions.

Quantification of the FeO diffusion

In a thin section of a type B1 inclusion, it is usually possible to optically constrain the geometry of a spinel below the plane of the thin section and, if spinel grains are chosen based on geometry, the position of the section within the crystal can be constrained. The section of TS-34 we used is, however, too thick to allow transmitted light microscopy and grains in section were chosen for analysis based on size, not geometry. This made it difficult to obtain detailed modeling of the zoning. We can nevertheless draw order of magnitude conclusions, based on the exponential attenuation lengths calculated from the FeO profiles as illustrated in Figs. 1 and 2. The functions describing diffusion profiles are not simple exponentials, but an exponential is a zeroth order approximation to any of the more complex functional forms. We assume that transport within the spinel is rate limiting and, therefore, that FeO is relatively mobile within any alteration source. We also effectively assume that the surface concentration of FeO was constant while diffusion into the spinel was occurring. Sufficient conditions for this assumption to be true are that alteration required for access of Fe to spinel surfaces be essentially complete prior to significant diffusion in spinel and that the diffusion occurred over a narrow temperature range.

We fit FeO concentrations, $C(x)$, along each FeO profile through an unweighted regression for the equation $C(x) = C_o + C_1\exp(-x/x_o)$. The constant C_o represents an upper bound on the concentration of FeO in the "primary" spinel as it existed prior to the event that generated the observed zoning, perhaps a residual from the last melting event in which the spinel crystallized. It is a maximum because the plane of the thin section may not, and generally will not, intersect the point of lowest concentration for the crystal. The exponential term represents FeO derived from diffusion into the crystal from grain surfaces. C_1 is a measure of the source strength, i.e., the amount of FeO in the alteration phases from which FeO has diffused into the spinel.

In Fig. 6, we show values of C_o and x_o for FeO profiles in spinel. The best-fit values for C_o in sutured pair A4 (–0.2) was below zero, which is physically unrealistic, and may reflect geometric complexities related to the suturing. Forcing $C_o = 0.00$, leads to a similar quality of fit. Excluding A4, values for C_o are in the range 0.01–0.07 wt%, consistent with the lowest

values, 0.03–0.07 (Connolly et al. 2003), for single grain analyses from various regions of TS-34 and in spinels from a lightly altered CAI from Leoville. It is possible that TS-34 experienced a thermal event leading to Fe diffusion comparable to that observed in Leoville that was partially overprinted by a later, more intense, episode. The iron data in TS-34 spinels may present another line of evidence for multiple alteration/oxidation events affecting CAIs (e.g., Beckett et al. 2000; Connolly et al. 2003; MacPherson and Davis 1993).

The attenuation length, x_o, is a measure of the homogenization distance for diffusion. The average of our profiles leads to x_o ~8 μm, and we adopt this as a representative value for the individual spinel grains. The lack of a consistent geometrical context for the spinel grains in this study, and the apparently variable nature of sources, makes it difficult to establish orientation of the sectioned spinels and effective diffusion distances for individual grains. For distances that are large compared to the size of the source regions, however, and for a fixed temperature, T, the exponential attenuation length, x_o, of the FeO profile can, as an order of magnitude approximation, be equated to $2\sqrt{D(T)t}$ where D is the diffusion coefficient and t the isothermal heating duration. Where there is an unobserved extended source geometry, especially from above or below the plane of the section, or where there are multiple sources to a measured profile, the inferred attenuation length will tend to be high (i.e., lower values tend to be better estimates). The tendency for sutured grains to yield relatively high values of x_o may be partly related to complex source geometries. This is almost certainly the case for A4.

Time Scales

Our model is that the observed FeO profiles in TS-34 spinels are produced by FeO-MgO interdiffusion. The introduction of FeO onto spinel grain boundaries may have occurred directly through vapor transport or indirectly by activation of local sources such as opaque assemblages. Since the last alteration event occurred well after crystallization of the primary igneous phases (Davis et al. 1994; Fagan et al. 2006), Fe zoning refers to heating and cooling during and following alteration rather than cooling immediately after partial melting of the inclusion. We take the total possible temperature range for alteration to be 400–1000 °C, although as noted above, the actual temperature range was probably much more restrictive. FeO diffusion in spinel becomes extremely sluggish below 400 °C, based on the diffusivities of Liermann and Ganguly (2002), and partial melting, leading to the destruction of alteration products will occur at temperatures not far above 1000 °C. We adopt $x_o = 8$ μm = $2\sqrt{D(T)t}$ as a representative value in an isothermal approximation, as shown in Fig. 7a. For peak temperatures in the range of 600–700 °C, times scales were in the range of years to decades. To the extent that presently fashionable
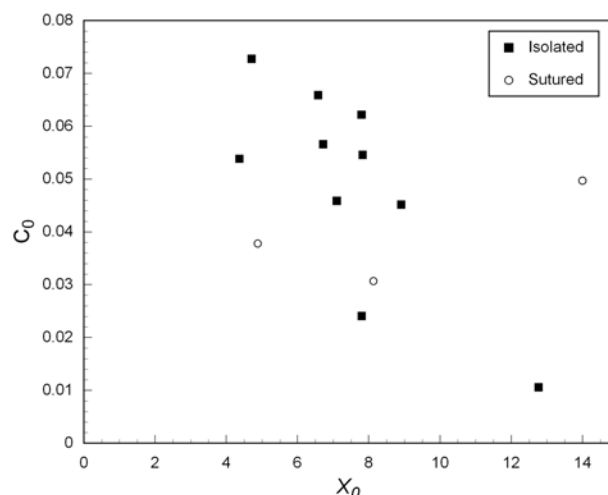

Fig. 6. Values of C_o as a function of x_o for profiles in isolated (closed symbols) and sutured (open symbols) spinel grains wholly included in either melilite/alteration products or clinopyroxene. The point for A4, which plots at 12.7, 0 is not shown (see text).

views on CAI formation time scales are correct and that these times are less than 10^6 yr, the temperature of CAI alteration is constrained to be greater than about 350 °C. If the time scale is set at about 100 days by the presence of ^{7}Be (Chaussidon et al. 2006) then CAI alteration temperatures would have been around 900 °C, which is facially inconsistent with thermometry estimates based on the alteration phases. The Be isotopic data refer, however, to melilite and fassaite, the principle hosts for Be. Diffusivities of Be and/or Li (^{7}Li is the daughter product of ^{7}Be decay) in these phases may be much smaller than those of Fe in spinel, leading to higher closure temperatures.

Figure 7a was constructed assuming that all diffusion occurred at a single temperature. We can also cast the diffusion problem in terms of a thermal history in which the inclusion is heated instantaneously to a maximum temperature T_o followed by exponential cooling with $T(t) = T_o e^{-at}$, where α is the fractional cooling rate. Following Kaiser and Wasserburg (1983), we obtain a solution to the one-dimensional diffusion equation by instituting a change of variables,

$$\tau(t) = \int_0^1 D(t^{'})dt^{'}, \qquad (1)$$

which leads to a revised homogenization equation of x_o ~$2\sqrt{\tau(t)}$. For exponential cooling, Kaiser and Wasserburg (1983) show that $(\tau)\infty \cong RD(T_o)T_o^2/rQ$, where R is the gas constant, r and $D(T_o)$ to the cooling rate and diffusivity at T_o, and Q the activation energy for diffusion. Figure 7b shows initial cooling rates as a function of T_o for an attenuation distance of 8 μm. Figure 7c shows thermal histories. For peak temperatures of 600–700 °C, initial cooling rates were
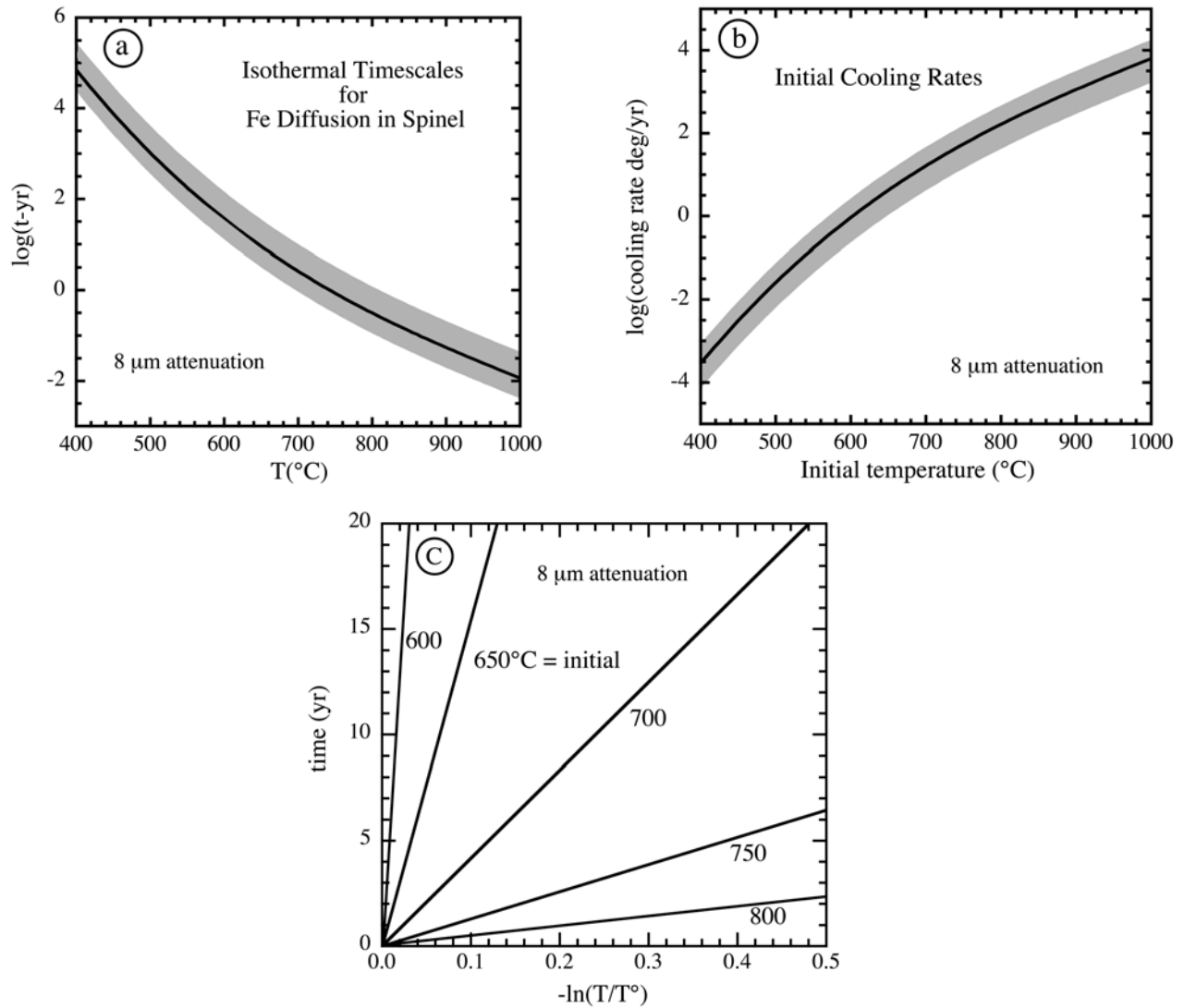
Fig 7. TS-34 spinel FeO diffusion using diffusion data of Liermann and Ganguly (2002) corrected to 1 bar and an 8 μm attenuation length.
a) Isothermal diffusion as a function of time and temperature. The shaded region surrounding the solid line bounds 5 and 15 μm attenuation
lengths. b) Initial cooling rates for exponential cooling from an initial temperature. The shaded region surrounding the solid line bounds 5 and
15 μm attenuation lengths. c) Thermal history for exponential cooling from an initial temperature T_0. Initial temperatures are indicated
adjacent to each line.

roughly 1–20 °C/yr and temperatures exceeded 400 °C for
20–250 yr. Even though these calculations are only semi-
quantitative, they imply that the thermal event associated with
the introduction of Fe into Allende CAIs was relatively brief.

Armstrong et al. (1987) performed a detailed study of a
region near a millimeter-size sulfide-rich Fremdling (Zelda)
in the type B1 CAI, Egg 3. Some spinels (A,B) in the vicinity
of Zelda (see also their Fig. 3) show large correlated
enrichments in Fe, V, and Cr, clearly associated with the
alteration event that produced Zelda. Zelda was interpreted as
being formed by sulfidization of a metal+V-rich magnetite
precursor with equilibration temperatures in the 600–800 °C
range. The FeO profile in spinel A near Zelda corresponds to
an exponential attenuation length of ~10 μm, which is

consistent with the upper end of the range observed for
individual crystals in this study (Fig. 6). An FeO abundance
profile extending away from an embayed opaque assemblage
in Armstrong et al.'s spinel C from the type B1 CAI 5241
(their Fig. 21b) also closely resembles what we observe in
TS-34. A second opaque assemblage included in spinel C that
has a clinopyroxene rim did not produce a FeO gradient
suggesting that oxidation/sulfidation did not occur through
the clinopyroxene rim. Armstrong et al. (1987) interpret their
spinel A diffusion profile as indicating diffusion at ≈1140 °C
for ≈2500 s, which would be consistent with production
during or shortly after crystallization of igneous phases,
provided the CAI was rapidly quenched from igneous
temperatures and never reheated. The diffusion coefficients of

Freer and O'Reilly (1980) used by Armstrong et al. (1987) were, however, obtained from a fine-grained sample in which grain boundary and, possibly, vapor transport contributed to extremely fast diffusion. Volume diffusion coefficients (Liermann and Ganguly 2002), which are the relevant parameters for modeling diffusion profiles in CAI spinels, are slower by about three orders of magnitude. Given relatively fast cooling rates for type B CAIs (MacPherson et al. 1984; Stolper and Paque 1986), an igneous origin for the Fe variations in spinel appears implausible. The 600–800 °C magnetite/sulfide equilibration temperature inferred by Armstrong et al. for equilibration of phases in the opaque assemblages would, as a peak temperature for alteration processes, correspond to Fe diffusion time scales of years to hundreds of years (Fig. 7).

The above discussion is fairly consistent in indicating an alteration time scale of years to centuries. It is possible that observed Li isotopic variations and the inferred presence of [7]Be (Chaussidon et al. 2006) would contradict this conclusion but data on Li and Be diffusion in CAI phases would be required to address this further.

Editorial Handling—Dr. Christine Floss

REFERENCES

Armstrong J. T., El Goresy A., and Wasserburg G. J. 1985. Willy: A prize noble Ur-Fremdling—Its history and implications for the formation of Fremdlinge and CAI. *Geochimica et Cosmochimica Acta* 49:1001–1022.

Armstrong J. T., Hutcheon I. D., and Wasserburg G. J. 1987. Zelda and company: Petrogenesis of sulfide-rich Fremdlinge and constraints on solar nebula processes. *Geochimica et Cosmochimica Acta* 51:3155–3173.

Barber D. J., Martin P. M., and Hutcheon I. D. 1984. The microstructure of minerals in coarse-grained Ca-Al-rich inclusions from the Allende meteorite. *Geochimica et Cosmochimica Acta* 48:769–783.

Beckett J. R., Simon S. B., and Stolper E. 2000. The partitioning of Na between melilite and liquid: Part II. Applications to type B inclusions from carbonaceous chondrites. *Geochimica et Cosmochimica Acta* 64:2519–2534.

Blum J. D., Wasserburg G. J., Hutcheon I. D., Beckett J. R., and Stolper E. M. 1989. Origin of opaque assemblages in C3V meteorites: Implications for nebular and planetary processes. *Geochimica et Cosmochimica Acta* 53:543–556.

Burnett D. S., Paque J. M., and Beckett J. R. 2004. Zoning patterns in spinel from type B Ca-Al-rich inclusions: Constraints on subsolidus thermal history (abstract #1253). 35th Lunar and Planetary Science Conference. CD-ROM.

Caillet C., MacPherson G. J., and Zinner E. K. 1993. Petrologic and Al-Mg isotopic clues to the accretion of two refractory inclusions onto the Leoville parent body: One was hot, the other wasn't. *Geochimica et Cosmochimica Acta* 57:4725–4743.

Chaussidon M., Robert F., and McKeegan K. D. 2006. Li and B isotopic variations in an Allende CAI: Evidence for the in situ decay of short-lived [10]Be and for the possible presence of the short-lived nuclide [7]Be in the early solar system. *Geochimica et Cosmochimica Acta* 70:224–245.

Connolly H. C. and Burnett D. S. 1999. A study of the minor element concentrations of spinels from two type B calcium-aluminum-rich inclusions: An investigation into potential formation conditions of calcium-aluminum-rich inclusions. *Meteoritics & Planetary Science* 34:829–848.

Connolly H. C., Burnett D. S., and McKeegan K. D. 2003. The petrogenesis of type B1 Ca-Al-rich inclusions: The spinel perspective. *Meteoritics & Planetary Science* 38:197–224.

Davis A. M., Simon S. B., and Grossman L. 1994. Alteration of Allende type B1 CAIs: When, where and how (abstract). 25th Lunar and Planetary Science Conference. pp. 315–316.

El Goresy A., Nagel K., and Ramdohr P. 1978. Fremdlinge and their noble relatives. Proceedings, 9th Lunar Science Conference. pp. 1279–1303.

Fagan T. J., Guan Y., and MacPherson G. J. 2006. Al-Mg isotopic constraints on alteration of Allende Ca-Al-rich inclusions (abstract #1213). 37th Lunar and Planetary Science Conference. CD-ROM.

Freer R. and O'Reilly W. 1980. The diffusion of Fe^{+2} ions in spinels with relevance to the process of maghematization. *Mineralogical Magazine* 43:889–899.

Hutcheon I. D. and Newton R. C. 1981. Mg isotopes, mineralogy, and mode of formation of secondary phases in C3 refractory inclusions (abstract). 12th Lunar and Planetary Science Conference. pp. 491–493.

Kaiser T. and Wasserburg G. J. 1983. The isotopic composition and concentration of Ag in iron meteorites and the origin of exotic silver. *Geochimica et Cosmochimica Acta* 47:43–58.

Krot A. N., Scott E. R. D., and Zolensky M. E. 1995. Mineralogical and chemical modification of components in CV3 chondrites: Nebular or asteroidal processing? *Meteoritics* 30:748–775.

Kurat G., Hoinkes G., and Fredriksson K. 1975. Zoned Ca-Al-rich chondrule in Bali: New evidence against the primordial condensation model. *Earth and Planetary Science Letters* 26:140–144.

Liermann H.-P. and Ganguly J. 2002. Diffusion kinetics of Fe^{2+} and Mg in aluminous spinel: Experimental determination and applications. *Geochimica et Cosmochimica Acta* 66:2903–2913.

MacPherson G. J. and Davis A. M. 1993. A petrologic and ion microprobe study of a Vigarano type B refractory inclusion: Evolution by multiple stages of alteration and melting. *Geochimica et Cosmochimica Acta* 57:231–243.

MacPherson G. J. and Grossman L. 1981. A once-molten, coarse-grained, Ca-rich inclusion in Allende. *Earth and Planetary Science Letters* 52:16–24.

MacPherson G. J., Paque J. M., Stolper E., and Grossman L. 1984. The origin and significance of reverse zoning in melilite from Allende type B inclusions. *Journal of Geology* 92:289–305.

MacPherson G. J. 2004. Calcium-aluminum-rich inclusions in chondritic meteorites. In *Meteorites, Comets, and Planets*, edited by Holland H. D. and Turekian K. K. Treatise on Geochemistry, vol. 1. Amsterdam, The Netherlands: Elsevier Pergamon. pp. 201–246.

MacPherson G. J., Wark D. A., and Armstrong J. T. 1988. Primitive material surviving in chondrites: Refractory inclusions. In *Meteorites and the early solar system,* edited by Kerridge J. F. and Matthews M. S. Tucson, Arizona: The University of Arizona Press. pp. 746–807.

McGuire A. V. and Hashimoto A. 1989. Origin of zoned fine-grained inclusions in the Allende meteorite. *Geochimica et Cosmochimica Acta* 53:1123–1133.

Meeker G. P., Wasserburg G. J., and Armstrong J. T. 1983. Replacement textures in CAI and implications regarding planetary metamorphism. *Geochimica et Cosmochimica Acta* 47: 707–721.

Nomura K. and Miyamoto M. 1998. Hydrothermal experiments on alteration of Ca-Al-rich inclusions (CAIs) in carbonaceous chondrites: Implication for aqueous alteration in parent asteroids. *Geochimica et Cosmochimica Acta* 62:3575–3588.

Paque J. M., Lofgren G. E., and Le L. 2000. Crystallization of calcium-aluminum-rich inclusions: Experimental studies on the effects of repeated heating events. *Meteoritics & Planetary Science* 35:363–371.

Paque J. M., Burnett D. S., and Beckett J.R. 2005. CAI thermal history constraints from spinel: Ti zoning profiles and melilite boundary clinopyroxenes (abstract #1809). 36th Lunar and Planetary Science Conference. CD-ROM.

Steele I. M., Peters M. T., Shaffer E. E., and Burnett D. S. 1997. Minor element partitioning and sector zoning in synthetic and meteoritic anorthite. *Geochimica et Cosmochimica Acta* 61:415–423.

Stolper E. 1982. Crystallization sequences of Ca-Al-rich inclusions from Allende: An experimental study. *Geochimica et Cosmochimica Acta* 46:2159–2180.

Stolper E. and Paque J. M. 1986. Crystallization sequences of Ca-Al-rich inclusions from Allende: The effects of cooling rate and maximum temperature. *Geochimica et Cosmochimica Acta* 50: 1785–1806.

Sutton S. R., Simon S., Grossman L., Delaney J. S., Beckett J., Newville M., Eng P., and Rivers P. E. 2002. Evidence for divalent vanadium in Allende CAI fassaite and implications for formation conditions (abstract #1907). 33rd Lunar and Planetary Science Conference. CD-ROM.

Taylor D. J. and McKeegan K. D. 2004. Further investigations of minor element distributions in spinels in type B CAIs (abstract #1958). 35th Lunar and Planetary Science. CD-ROM.

Wark D. A. 1981. Alteration and metasomatism of Allende Ca-Al-rich inclusions (abstract). 7th Lunar Science Conference. pp. 1145–1147.

Wark D. and Boynton W. V. 2001. The formation of rims on calcium-aluminum-rich inclusions: Step I—Flash heating. *Meteoritics & Planetary Science* 36:1135–1166.

Wark D. A. and Lovering J. F. 1977. Marker events in the early evolution of the solar system: Evidence from rims on Ca-Al-rich inclusions in carbonaceous chondrites. Proceedings, 8th Lunar Science Conference. pp. 95–112.